Z. Phys. C – Particles and Fields 45, 529–537 (1990)

Zeitschrift für Physik C Particles and Fields

Transverse energy production in the target fragmentation region in ^{16}O-nucleus reactions at 60 and 200 A GeV

WA 80-Collaboration

R. Albrecht[1], T.C. Awes[2], C. Baktash[2], P. Beckmann[3], F. Berger[3], R. Bock[1], G. Claesson[5], G. Clewing[3], L. Dragon[3], A. Eklund[5], R.L. Ferguson[2], A. Franz[4,a], S. Garpman[5], R. Glasow[3], H.Å. Gustafsson[5], H.H. Gutbrod[1], J. Idh[5], P. Jacobs[4], K.H. Kampert[3], B.W. Kolb[1], P. Kristiansson[4,5], I.Y. Lee[2], H. Löhner[3,b], I. Lund[1], F.E. Obenshain[2,a], A. Oskarsson[5], I. Otterlund[5], T. Peitzmann[3], S. Persson[5], F. Plasil[2], A.M. Poskanzer[4], M. Purschke[3], H.G. Ritter[4], S. Saini[2], R. Santo[3], H.R. Schmidt[1], T. Siemiarczuk[1,c], S.P. Sorensen[2,a], E. Stenlund[5], M. Tincknell[2], G.R. Young[2]

[1] Gesellschaft für Schwerionenforschung, Darmstadt, Federal Republic of Germany
[2] Oak Ridge National Laboratory, Oak Ridge, Tenn., USA
[3] University of Münster, Münster, Federal Republic of Germany
[4] Lawrence Berkeley Laboratory, Berkeley, Calif., USA
[5] University of Lund, Lund, Sweden

Received 21 July 1989

Abstract. Charged pion yields and transverse energies of baryons are measured for the reaction ^{16}O + Cu, Ag, Au at 60 and 200 A GeV bombarding energy in the target fragmentation region employing the Plastic Ball detector. Only little dependence of the measured quantities on the bombarding energy is found. The data are compared with the multi-chain fragmentation model of Ranft. As a result it turns out that a leading order formation zone cascade is not sufficient to explain the baryon yield and the transverse energies of baryons in the target fragmentation region.

I Introduction

Nucleon-nucleus and nucleus-nucleus collisions at ultrarelativistic energies offer the interesting opportunity to investigate the space-time development of the formation of secondary hadrons because the nucleons in a nucleus serve as detectors of the products of the initial collision.

The various available string models [1–6] reproduce rather successfully the particle and transverse energy production [7–15] at mid and forward rapidities. It has, however, been observed in hadron-nucleus collisions [9, 16, 17] that an excess of particles over the model predictions in the backward rapidity region. Furthermore, pseudorapidity distributions of charged particles [18–20] show, unlike the distributions at forward rapidity, a strong dependence on the target mass.

The standard, qualitative explanation of these observations is a cascading mechanism, where the produced secondaries from the primary collisions reinteract with the surrounding target matter. It is still an open question whether experimental data can be fully described by this intra-nuclear cascade reaction mechanism. This is partly due to the lack of exclusive experimental data in the target fragmentation region, but, on the other hand, it was only recently that string models have been combined with intra-nuclear cascading [2, 21, 22]. In these models a phenomenological parameter, τ, which has to be determined from experiment, controls the formation time of secondaries and hence the strength of the coupling of the participant matter to the target spectator matter. Measurements in the target fragmentation region can therefore also serve to extract fundamental information about the time scale of hadron creation.

A more unconventional mechanism to couple the projectile to the target is a shock wave [23, 24], as already early suggested by Belen'kji and Landau [25],

[a] University of Tennessee, Knoxville, Tenn., USA
[b] University of Groningen, Groningen, The Netherlands
[c] Institute for Nuclear Studies, Warsaw, Poland

Glassgold et al. [26] and later by Baumgardt et al. [27]. A description in terms of hydrodynamic shock compression of nuclear matter has been very successful in explaining experimental findings like collective sideward flow at the much lower bombarding energies around 0.5 A GeV [28–30]. A comparison of a 3-dimensional 1-fluid hydrodynamical calculation for O+Pb at 60 and 200 A GeV bombarding energy [24] with our data [31] seems, however, not yet conclusive: while the calculated rapidity distribution of baryons agrees well with the data at 60 A GeV, a discrepancy occurs at 200 A GeV. In the latter case the model predicts a too high rapidity shift of the target baryons.

The present data were measured employing the Plastic Ball detector [32]. This detector, which was formerly employed as a 4 π-detector at the BEVALAC at Berkeley, has been incorporated into the WA 80 experiment [33] in order to cover the target rapidity region. Its capability to identify particles and to measure their energies gives the possibility to study the target fragmentation region in great detail. In this paper we shall mainly focus on baryon measurements in the target rapidity region and in particular onto their transverse energies. We shall compare our experimental result with model calculations done with Ranft's multi-chain fragmentation model (MCFM) [2, 13], which is modified by a leading order formation zone cascade. The possibility to determine the formation time τ shall be discussed.

II Experimental setup

The data were taken with the WA 80 setup [33] using the 60 and 200 A GeV ^{16}O beam delivered from the CERN SPS. The typical beam level was 2×10^6 ions per beam spill. The ^{16}O-ions were identified with thin, total-reflection quartz Cerenkov counters. The data were taken with a minimum bias trigger requiring: i) less than 88% of the full beam energy measured in a zero degree calorimeter (ZDC) [34]; ii) at least one charged particle recorded within a polar angle of $30° \geqq \vartheta \geqq 1°$.

The Plastic Ball [32] measures charged particles emitted in the angular range $160° \geqq \vartheta \geqq 30°$ ($-1.7 \leqq \eta \leqq 1.3$). In its present configuration, it consists of 655 ΔE-E modules arranged in a sphere. The modules are capable of identifying charged π's, protons, deuterons, tritons and ^{3,4}He. Protons up to 240 MeV are stopped in the 35.6 cm long plastic scintillators. The measured pions are predominantly minimum ionizing. Therefore the Plastic Ball determines only the yield of the charged pions, but does not measure their energy. The ΔE counter, a 4 mm CaF_2 crystal, allows, to some extent, an extension of energy measurements of protons based on the ΔE signal alone. In the present data set proton energies were determined up to about 300 MeV. The low energy cut-off depends (i) on the energy loss in the target foil, which is a function of the energy and the angle ϑ of the particles, and (ii) on the particles stopping in the ΔE-counter. In order to minimize the absorption of slow particles thin targets were chosen: 200 mg/cm^2 of Cu and Ag, and 250 mg/cm^2 of Au. For the same reason the target vacuum chamber was made of 135 mg/cm^2 of aluminium.

III Data analysis and Monte Carlo corrections

The copious pion production in central heavy-ion collisions at ultrarelativistic energies leads to a non-negligible multiple-hit probability in the Plastic Ball detector – in particular at the more forward angles. The multiple-hit correction for charged particles can be estimated analytically. However, in order to correct spectra and yields of identified particles an involved Monte Carlo calculation is required. The complexity of the problem can be conceived considering the following example: The measured yield of, e.g. protons, of a certain energy consists of "true" and "false" protons, the false ones originating from double- or multiple hits of a single detector module by mostly pions, δ-electrons and neutral particles. The probability for the occurrence of the false, background protons of a certain energy depends both on the yield and the spectral distribution of pions, δ-electrons and neutral particles. For the latter ones the response of the plastic scintillator to neutral particles has to be taken into account. While this process increases the apparent yield of measured protons over the true yield, it is, on the other hand, diminished by multiple hits of protons with other kinds of particles. The influence of this second process depends again on the yield and spectral distribution of the particles.

Our approach to simulate the response of the Plastic Ball by means of Monte Carlo calculations in a high multiplicity environment is as follows: Several low multiplicity events ($N_{\text{charged}} < 25$), as measured in the Plastic Ball, are convoluted under the condition that the multiplicity distribution $\sigma(N)$ of a central event is reproduced. The underlying assumptions are that the low multiplicity samples consist of well identified particles and that the phase space distribution of particles from a low multiplicity event, i.e. a peripheral collision, is not too different from a central one. While the first assumption can be verified directly by looking at the measured ΔE-E spectrum, the second one is not evident a priori. However, the main source hampering the identification of baryons are multiple hits of charged pions and γ's from π^0-decay.

The production of these particles is rather successfully described by models based on independent nucleon-nucleon collisions [14]. This suggests that also the second assumption is valid to a high degree.

Our Monte Carlo, having as input events consisting of well identified particles, yields both the background of the baryon distribution as well as a correction factor due to multiple hits. The background contribution below the relatively sharp peak resulting from minimum ionizing charged pions is negligible and therefore not explicitly calculated, i.e. $N_{\text{bgnd}}^{\text{MC}}$ entering (1) and (2) below is assumed to be zero for pions. The actual calculation of the correction is done in two dimensions, i.e. as a function of angle and energy. The formula used to reconstructed the "true" yields of particles, N_{true}, is

$$N_{\text{true}} = \frac{N^{\text{exp}} - N_{\text{bgnd}}^{\text{MC}}}{\varepsilon} \tag{1}$$

with the efficiency ε given by

$$\varepsilon = \frac{N^{\text{MC}} - N_{\text{bgnd}}^{\text{MC}}}{N_{\text{true}}^{\text{MC}}}. \tag{2}$$

N^{exp} is the experimentally measured yield and N^{MC} and $N_{\text{bgnd}}^{\text{MC}}$ are the results of the Monte Carlo simulation for the measured yield and the background contribution, respectively. $N_{\text{true}}^{\text{MC}}$ is the Monte Carlo result for a detector of infinite granularity, i.e. no double hits.

Figure 1 shows a result of the Monte Carlo calculations. Shown are the efficiencies ε for measuring a proton or a charged pion, respectively, as a function of the pseudorapidity η for a central collision of O+Au at 200 A GeV. It can be seen that the efficiency to detect a proton in the most forward ring of modules ($1.0 < \eta \leqq 1.3$) of the plastic ball is only $\approx 20\%$ and hence the correction is correspondingly large. We will therefore present our results on baryons in the limited range of $-1.7 \leqq \eta \leqq 0.6$, where the efficiency is $> 60\%$. For the same reason results on pion yields will be presented for $-1.7 \leqq \eta \leqq 1.0$.

The particle identification window in the ΔE-E plane for minimum ionizing pions was chosen such that double hits with neutral particles or not too energetic δ-electrons will still fall into the pion window. For baryons, on the other hand, where the kinetic energy is determined and isotope separation is required, the width of the particle identification band has to be sufficiently narrow, making the baryon yield more susceptible to double hits losses. For these reasons the efficiency ε for measuring baryons is always smaller than for measuring pions and reaches only about 80% at backward angles, in contrast to a value close to 100% for pions.

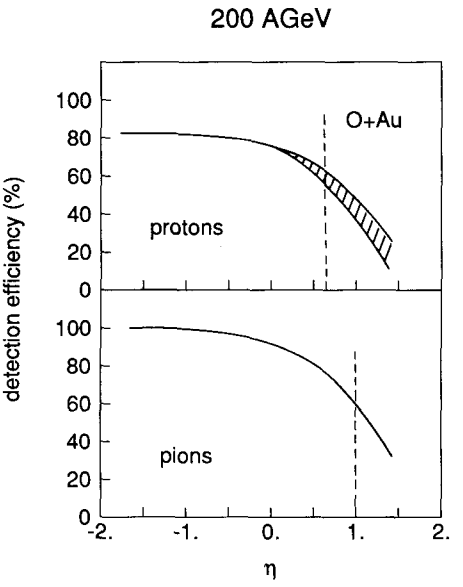

Fig. 1. Efficiencies for detecting a proton or a charged pion in a central collision O + Au at 200 A GeV as estimated from the Monte-Carlo calculation described in the text

The Monte Carlo calculation – a convolution of peripheral events done under the condition that the experimental *integral* distribution $\sigma(N)$ of a central event is reproduced – describes the measured *differential* distributions $dN/d\eta$ within $\pm 15\%$. Additionally, we have studied the effect of varying the background $N_{\text{bgnd}}^{\text{MC}}$, which enters (1) predominantly via the denominator $(N^{\text{MC}} - N_{\text{bgnd}}^{\text{MC}})$. The band in the upper graph of Fig. 1 represents the result of this estimate for the efficiency ε for protons. As can be seen the effect on ε becomes large for $\eta > 1$, where the "signal-to-background" ratio for protons is small. In our restricted range $-1.7 \leqq \eta \leqq 0.6$, however, the variation in ε is relatively small. We therefore take $\pm 15\%$ as a rough estimate of the systematic error of the correction to the data. The corresponding uncertainties for the calculation of baryon yields, transverse energies etc. are shown as error bars in the distributions or are listed in the tables. The statistical error is, except in the very tails of the distributions, always much smaller than the systematic one and is therefore, if not mentioned otherwise, not considered.

Furthermore it is found that for proton energies above 300 MeV the background from pions becomes intolerably large: therefore we restrict proton identification to the window $20\ \text{MeV} < E_{\text{proton}} < 300\ \text{MeV}$*. Figure 2 shows a particle identification spectrum for

* Apparent differences from preliminary results published as proceedings of the 6th International Conference on Ultra-Relativistic Nucleus-Nucleus Collisions-Quark Matter 1987 in [31] are mainly due to this restriction in the proton identification window

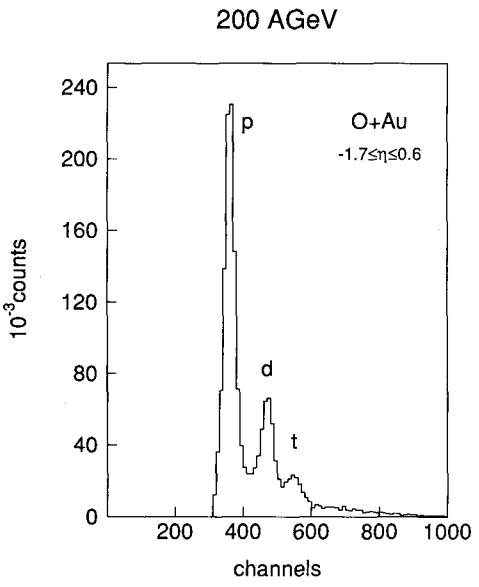

Fig. 2. Particle identification spectrum for baryons for central collisions O+Au at 200 A GeV. The Monte-Carlo simulated background due to multiple hits has been subtracted

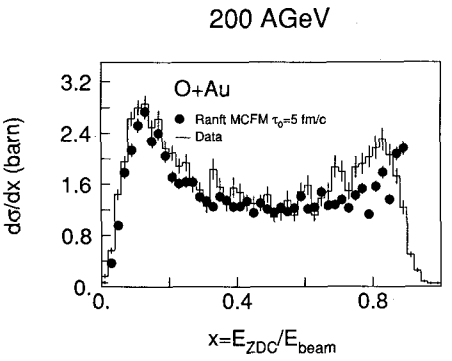

Fig. 3. Comparison of the energy spectrum obtained from Ranft's MCFM at $\Theta < 0.3°$ (filled circles) with the measured spectrum in the ZDC (histogram) for the reaction $^{16}O + Au$ at 200 A GeV

central O+Au collisions. The spectrum is integrated over the pseudorapidity and energy range $-1.7 \leqq \eta \leqq 0.6$ and 50 MeV $< E_{\text{nucleon}} <$ 150 MeV, respectively. It is corrected for background contributions due to multiple hits.

The data presented in this paper are characterized by the remaining energy of the projectile at small angles ($<0.3°$), as measured in the ZDC [34] of the WA 80-experiment. Central events at 200 A GeV bombarding energy were selected by requiring less than 20, 30 and 40% (12, 14 and 22% at 60 A GeV) of the full beam energy deposited in the ZDC for the reaction $^{16}O + Au$, Ag and Cu, respectively. All spectra shown in the paper are selected for central collisions employing the above critera. It should also be noted that we estimate the number of baryons as $(A/Z)p + 2d + 3(t + {}^3\text{He}) + 4\,{}^4\text{He}$, where the factor A/Z accounts for the unmeasured neutrons. A and Z are the target mass and charge, respectively.

When comparing with model data, the generated events are subjected to the same cuts and selections as the experimental ones, which are: i) the absorption of low energy particles in the target material; ii) the lower and upper energy detection thresholds for protons iii); the angular selection of $-1.7 \leqq \eta \leqq 0.6$ or 1.0, dependent on the particles considered; iv) the centrality selection via energy spectra at zero degrees as described above*.

* A FORTRAN subroutine to filter the output of simulations so that they can be compared with our data is available from the authors

Figure 3 compares the energy spectrum at $\Theta < 0.3°$ obtained from the generated events with the measured spectrum in the ZDC for the reaction $^{16}O + Au$ at 200 A GeV. The error shown is statistical only. The similarity of the spectra assures the same impact parameter range selection for both the experimental and simulated data. The effect of the acceptance cut of the plastic ball can, for example, be seen in Figs. 7 and 9.

IV Results

IV.1 Calorimeter-like E_t-distributions

Energy measurements in ultrarelativistic nucleus-nucleus collisions have so far mainly been carried out measuring the energy of particles deposited in a calorimeter [10–12, 15, 35]. The interest was hereby focused on the transverse energy $E_t \equiv \sum E_i \sin \vartheta_i$, where the sum extends over the calorimeter cells. In order to complement these measurements, which were done mostly at mid and forward rapidities (only NA 34 covers part of the target fragmentation region by measuring for $\eta \geqq -0.1$), the Plastic Ball data are analyzed in the same manner as would be obtained using a calorimeter. The inputs are the measured energy distribution of the baryons $dE_t^{\text{baryon}}/d\eta$ and the distribution $dN^{\pi}/d\eta$ of charged pions. π^0's are taken approximately into account by multiplying the charged pion distribution by 3/2. Particles with energies larger than 300 MeV are considered as pions. Pions are predominantly minimum ionizing and their energy is not measured in the Plastic Ball. The average transverse energy per pion $\langle E_t^{\pi}/\text{pion} \rangle$, where $E_t^{\pi} = \sin \vartheta \sqrt{(p^2 + m^2)}$, as a function of η is therefore taken from Ranft's MCFM and is shown in Fig. 4. The value of $\approx$360 MeV for $\eta > 0.5$ is roughly in agreement with experimental data measured in the region $2.0 \leqq \eta \leqq 4.2$ [20]. The uncertainty due to these assumptions

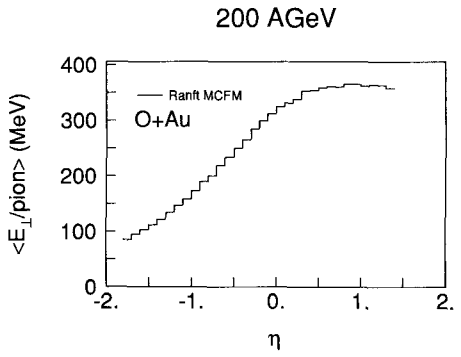

Fig. 4. Average (calorimetric) transverse mass of pions as calculated within Ranft's MCFM as a function of the pseudorapidity η. These values are used to estimate the integrated transverse energy E_t from the measured pion yields

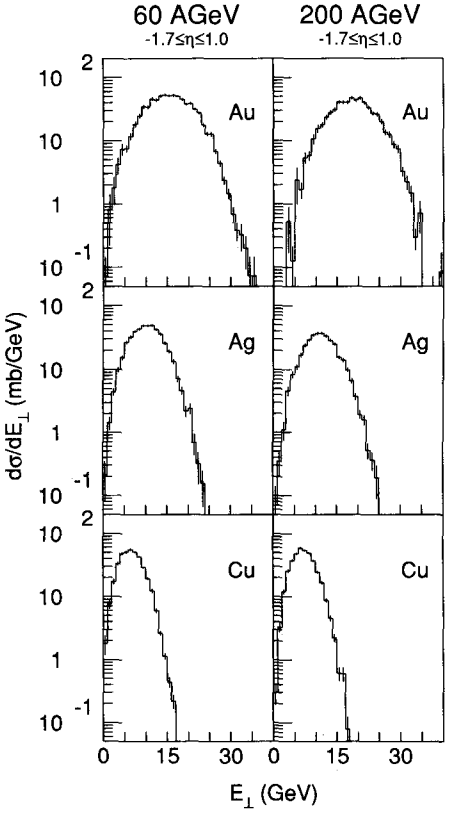

Fig. 5. Transverse energy spectra measured in the plastic ball in the range $-1.7 \leqq \eta \leqq 1.0$

should be compared with the typical resolution of $35\%/\sqrt{E}$ of the best sampling calorimeters, which results in a particularly poor performance for the soft particles in the target fragmentation region.

Figure 5 shows the so obtained transverse energy distributions for central collisions of O + Au, Ag and Cu in the range* $-1.7 \leqq \eta \leqq 1.0$ for both 60 and 200 A GeV bombarding energy. The error bars represent the statistical error. The numerical values of the average E_t of a central collision as well as the uncertainty due to the systematic error are shown in Table 1. The target dependence – $\langle E_t^{\text{central}} \rangle \propto A_{\text{target}}^{\alpha}$ – is $\alpha \approx 0.75$ for 60 and ≈ 0.84 for 200 A GeV. In order to allow comparison with transverse energies from baryons alone, on which we will report further below, the values of $\langle E_t^{\text{central}} \rangle$ in the more restricted η-range $-1.7 \leqq \eta \leqq 0.6$ are also given in Table 1. Further below, we shall see to which fraction the slope parameter α is due to transverse energy carried by mesons and by baryons. However, we already see that the increase of $\langle E_t^{\text{central}} \rangle$ in the target fragmentation region is much stronger than the $\propto A_{\text{target}}^{1/3}$ dependence one would expect from scaling with the target nucleus thickness. Furthermore, we want to emphasize that the transverse energy observed at backward rapidities amounts to roughly 20% of the E_t measured in the range $2.4 \leqq \eta \leqq 5.5$ [10].

Figure 6 shows the corresponding distributions $dE_t/d\eta$. As for the E_t-distributions, only little dependence on the bombarding energy is observed. Distributions of this kind, as well as integrated yields as in Fig. 5 have been used to extract information about the amount of cascading [2, 3, 11, 13] in nucleon-nucleus and nucleus-nucleus collisions. Since, in our case, these spectra are somewhat model dependent, since they do contain the average transverse energy per pion taken from Ranft's MCFM, they are not compared with the model predictions.

Table 1a, b. Average transverse energies and slope parameters α obtained from $\langle E_t \rangle \propto A_{\text{target}}^{\alpha}$ for 60 **a** and 200 **b** A GeV bombarding energy. The values are given in GeV. The slope parameter given in brackets is from $\langle E_t^{\text{baryon}} \rangle \propto A_{\text{spectators}}^{\alpha}$ as described in the text

Target	η	Cu	Ag	Au	α
a					
$\langle E_t \rangle$	$[-1.7, 1.0]$	6.7 ± 1.0	10.4 ± 1.6	15.6 ± 2.3	0.75
$\langle E_t \rangle$	$[-1.7, 0.6]$	3.1 ± 0.5	5.0 ± 0.7	7.8 ± 1.1	0.81
$\langle E_t^{\pi} \rangle$	$[-1.7, 0.6]$	2.3 ± 0.4	3.5 ± 0.5	5.0 ± 0.7	0.68
$\langle E_t^{\text{baryon}} \rangle$	$[-1.7, 0.6]$	0.8 ± 0.1	1.5 ± 0.2	2.8 ± 0.4	1.11 (0.95)
b					
$\langle E_t \rangle$	$[-1.7, 1.0]$	7.2 ± 1.1	11.3 ± 1.7	18.8 ± 2.8	0.84
$\langle E_t \rangle$	$[-1.7, 0.6]$	3.4 ± 0.5	5.3 ± 0.8	9.1 ± 1.4	0.87
$\langle E_t^{\pi} \rangle$	$[-1.7, 0.6]$	2.6 ± 0.4	3.8 ± 0.6	5.9 ± 0.9	0.72
$\langle E_t^{\text{baryon}} \rangle$	$[-1.7, 0.6]$	0.8 ± 0.1	1.5 ± 0.2	3.2 ± 0.5	1.22 (1.04)

* We use here the baryons up to $\eta = 1.0$; since the pions dominate the yield, the additional uncertainty remains relatively small

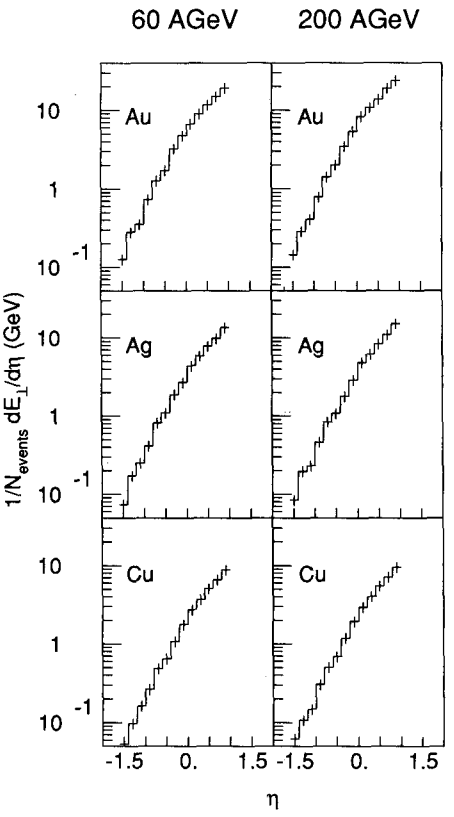

Fig. 6. Distribution of the transverse energy measured in the plastic ball as a function of the pseudorapidity η

In the following section we will discuss in detail the measured pion yields and baryonic component of these spectra. They will be compared with Ranft's MCFM in order to find out if an intra-nuclear cascade, combined with the concept of a formation zone for secondary hadrons is sufficient to describe the measured yields and transverse energies.

IV.2 Distributions from identified particles

IV.2.1 The concept of a formation zone intra-nuclear cascade. In his model Ranft has modified a dual parton Monte Carlo by a leading order formation zone cascade [2, 13], which couples the primary interaction zone to the spectator region. Secondary hadrons in the collisions are not formed instantaneously. In their rest frame they need a certain time distributed exponentially with average τ, which is called the formation time, before they are present as complete hadronic states. During this time the hadrons have a reduced probability for hadronic interactions inside the nucleus. This picture explains the absence of intra-nuclear cascading at large rapidities, where the hadrons, due to relativistic time dilation, are created outside of the nucleus. At lower rapidities, however, hadrons produced in primary collisions have the possibility to couple to the target spectator matter. A phenomenological parameter τ_0 is introduced which must be determined by comparison with experiment. The formation time in the laboratory is then given by

$$\tau_{\text{lab}} = \gamma_s \tau_s \tag{3}$$

where $\gamma_s = E_s/m_s$ is the Lorentz factor of the secondary, and

$$\tau_s = \tau_0 \frac{m_s^2}{m_s^2 + p_{ts}^2} \tag{4}$$

is the formation zone in the rest frame of the secondary produced particle*. The quantities p_{ts} and m_s are the transverse momentum and the mass of the secondary particle, respectively. The leading order cascade considers only secondary collisions of particles which are produced in the primary collision. It does not include the intranuclear cascade for all low-energy hadrons created in the secondary collisions, and so on.

Figure 7 shows a typical rapidity distribution of baryons as calculated with the model for central collisions of O+Au at 200 A GeV and a τ_0 of 5 and 100 fm/c, given by the dashed and solid curves, respectively. Only those baryons which are produced either in the primary collisions or by the cascade are shown, i.e. the integrated yield of baryons is always smaller than the sum of A_{target} and $A_{\text{projectile}}$. Three regions are clearly distinguishable: a) ≈ 16 baryons, – the projectile participants – can be found for $y > 3$; b) ≈ 41 baryons, – the target participants, – fall within $0.5 < y \leqq 3$; and c) the target fragmentation region for $y \leqq 0.5$. It is only in region c) where the baryon number depends substantially on the formation zone. The dashed-dotted histogram in Fig. 7 shows the baryon distribution for $\tau_0 = 5$ fm/c after taking the Plastic Ball acceptance into account. The main cause for this drastic reduction in the baryon number is, beside the angular cuts, the low energy cut-off of the Plastic Ball, which discriminates against the very soft target baryons predominantly present only in the model calculations.

IV.2.2 Pion yields. Figure 8 shows the distributions $dN^{\pi}/d\eta$ of charged pions. They are compared with calculations within Ranft's MCFM using two different values of τ_0 for the formation zone cascade: the

* It should be noted that in [13] the formation zone τ is introduced with a p_t dependence given in (4), therefore the parameter τ_0 of (4) differs from the formation zone parameter used in [2]. The factor $m_s^2/(m_s^2 + p_{ts}^2)$ increases the extracted τ_0 by a factor of 7.3, if one assumes a pion with $m_{ts} = 375$ MeV

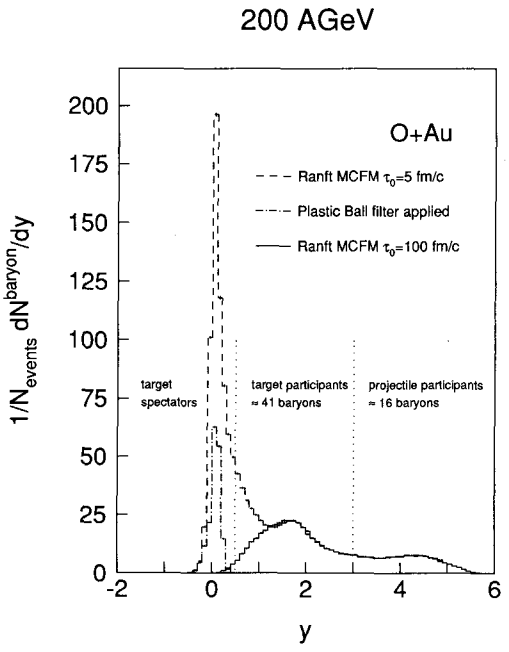

Fig. 7. The distribution of baryons as calculated within Ranft's MCFM as a function of the rapidity y for central collisions O+Au and a formation time parameter τ_0 of 5 (dashed curve) and 100 fm/c (solid curve). The dashed-dotted curve is obtained after filtering the model data ($\tau_0 = 5$ fm/c) with the plastic ball acceptance

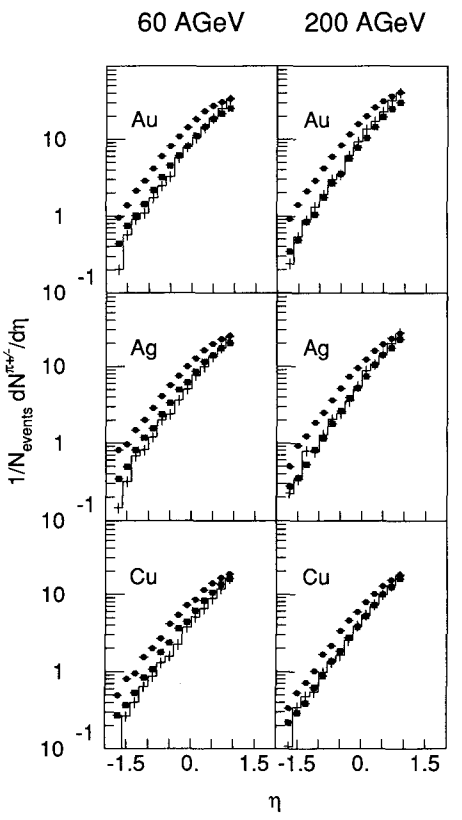

Fig. 8. Yield of charged pions as a function of the pseudorapidity η. The histogram represents the measured data, the circles and squares show calculations within Ranft's MCFM assuming a formation zone parameter τ_0 of 5 and 100 fm/c, respectively

circles and squares are for $\tau_0 = 5$ and 100 fm/c, respectively. At a formation time $\tau_0 = 100$ fm/c the particles materialize outside of the nucleus, i.e. they do not rescatter in the target spectator. As can be seen the pion yields can be described at both bombarding energies and for all target-projectile combination shown without the necessity to consider rescattering in the target. It is, however, evident that the pion yields are not a very sensitive tool for a determination of the formation time, since the choice of a relatively short formation time ($\tau_0 = 5$ fm/c) only slightly overpredicts the measured data. For comparison the experimental $\langle E_t^{\text{central, pion}} \rangle$ and the corresponding α-value in the range $-1.7 \leqq \eta \leqq 0.6$ are also given in Table 1.

IV.2.3 Baryon yields and transverse energy distributions. The yield of baryons at backward rapidities is expected be much more sensitive to cascading of secondary particles. As already pointed out in Sect. IV.2.1 the baryon yield resulting from the model calculation is strongly influenced by the low energy cutoff of the Plastic Ball. Figure 9 compares the momentum spectrum of protons from O+Au in the range $0.08 \leqq y \leqq 0.18$ with the calculated one for a formation time of $\tau_0 = 5$ fm/c. The error bars represent the statistical errors only. It turns out that the simulated proton momentum spectrum is much softer than the ex-

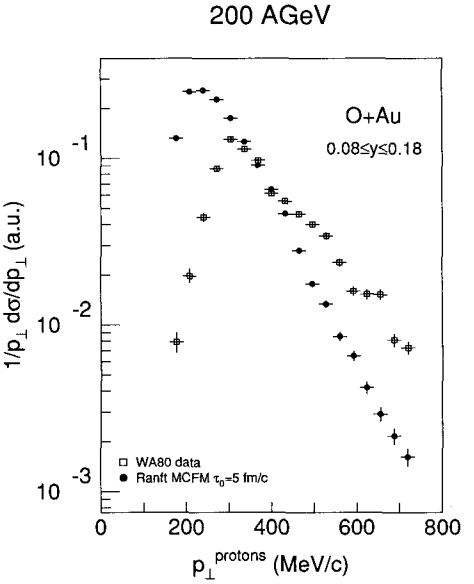

Fig. 9. Invariant cross section $1/p_t\, d\sigma/dp_t$ of protons in the range $0.08 \leqq y \leqq 0.18$. The open squares represent the measured data and the filled circles the calculations within Ranft's MCFM assuming a formation zone parameter $\tau_0 = 5$ fm/c

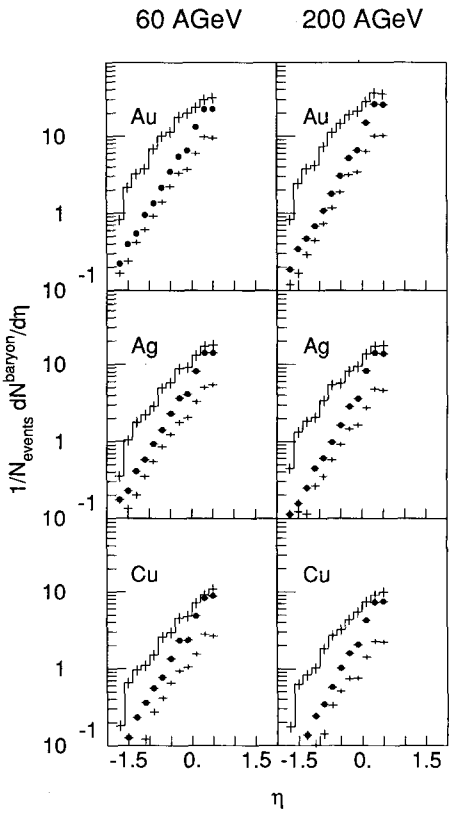

Fig. 10. Yield of baryons as a function of the pseudorapidity η. The histogram represents the measured data, the circles and crosses show calculations within Ranft's MCFM assuming a formation zone parameter τ_0 of 5 and 10 fm/c, respectively

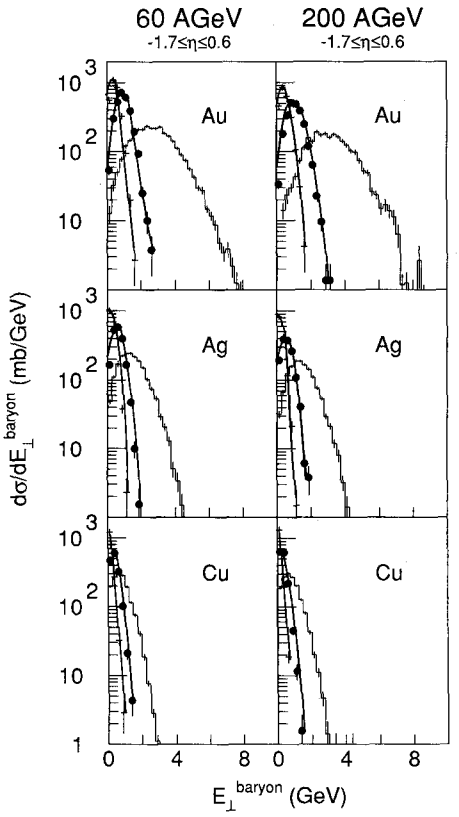

Fig. 11. Transverse energy spectra of baryons in the range $-1.7 \leqq \eta \leqq 0.6$. The histogram represents the measured data while the circles and crosses show calculations within Ranft's MCFM assuming formation zone parameters τ_0 of 5 and 10 fm/c, respectively. The solid lines are to guide the eye

perimental one. Hence the experimental proton yield is much less affected by the low energy cut-off than the model data, which are reduced by almost 50% when applying the Plastic Ball filter.

Figure 10 compares the $dN^{baryon}/d\eta$-distributions with the predictions of the model for $\tau_0 = 5$ and 10 fm/c. The model gives, as a consequence of the low energy cutoff, considerably fewer baryons than the data, even with the choice of a small formation zone parameter ($\tau_0 = 5$ fm/c). Furthermore, the shape of the spectrum is not described – in particular for $\eta < 0$ the discrepancy is large.

Figure 11 shows transverse energy distributions of baryons for O+Au, Ag and Cu in the range $-1.7 \leqq \eta \leqq 0.6$. The error bars represent the statistical errors. The numerical values of $\langle E_t^{central,\,baryon} \rangle$ as well as the uncertainty due to the systematic error are given in Table 1. The circles and crosses represent calculations for $\tau_0 = 5$ and 10 fm/c. In neither case are the data at all reproduced. The calculation for $\tau_0 = 10$ fm/c underestimates $\langle E_t^{central,\,baryon} \rangle$ by a factor of 5; for $\tau_0 = 5$ fm/c the data are still underestimated by a factor of 2. The target dependence, if parameterized with A_{target}^{α} gives $\alpha = 1.11$ for 60 and 1.22 for 200 MeV/nucleon incident energy, respectively. Since the systematic error will probably influence $\langle E_t \rangle$ for the different targets into the same direction it is not considered as a source of uncertainty for the extraction of α. Using a more realistic, but model dependent parameterization, namely $\langle E_t^{central,\,baryon} \rangle \propto A_{spectators}^{\alpha} = (A_{target} - A_{participants}^{\alpha})$ one obtains $\alpha = 0.95$ and 1.04 for the two bombarding energies, which might imply that the observed baryons arise dominantly from target spectator matter. The number of target participants is taken from Ranft's MCFM as outlined in Sect. IV.2 and is 22, 30 and 41 for Cu, Ag, and Au, respectively.

V Summary and conclusions

In summary we have measured pion yield and transverse energies of baryons in the target fragmentation region for the reactions $^{16}O + Au$, Ag, Cu at 60 and 200 A GeV bombarding energy. We have found only little difference for the above quantities at the two bombarding energies. This observation resembles the

limiting fragmentation behavior found for the cross sections of intermediate mass fragments ($A < 50$) produced in 60 and 200 A GeV ^{16}O collisions with ^{238}U [36]. In the case of pion production, however, the similarity of the yields at target pseudorapidities can be attributed to the different kinematics at the two bombarding energies: the η-distributions shift towards larger η with increasing incident energy giving about the same yields for $\eta < 1$ [37]. This might, on the other hand, also explain the similarity of baryon production at target rapidities, namely under the assumption that the target spectator baryons couple to the primary interaction zone via the pions.

The transverse energy for $\eta \leqq 1.0$ is about 20% of the E_t typically measured at mid rapidity in the range $2.4 \leqq \eta \leqq 5.5$ [10]. The E_t in the target region is decomposed into its pion and baryon component. It is found that about 30% of the transverse energy is carried by baryons (in the region $-1.7 \leqq \eta \leqq 0.6$). The slope parameter α describing the target mass dependence of E_t is an mixture of the strong target mass dependence of the baryon component and of the relatively weaker dependence of the pion component. The value of α for the baryon transverse energy is $\geqq 1$, which indicates a process where the whole target nucleus becomes excited during the passage of the projectile through the target nucleus.

We have compared the data with Ranft's MCFM. The pion yield at backward pseudo-rapidities can be satisfactorily reproduced without the necessity to invoke rescattering. On the other hand, we have shown, based on an energy measurement, that the target spectator baryons are not adequately described by the leading order formation zone cascade contained in the model. The transverse energy of baryons is, even for the small formation time parameter $\tau_0 = 5$ fm/c, underestimated by the model by more than a factor of two. The observation that the model fails to reproduce the proton momentum spectrum hence questions the possibility to extract the formation time from a comparison of this model with the measured baryon yields or transverse energy distributions.

It has to be left to further theoretical investigations if a full intra-nuclear cascade [22], which includes all subsequent collisions of hadrons created in turn in the secondary collisions and so on, will better agree with the data.

References

1. T.P. Pansart: Nucl. Phys. A461 (1987) 521c
2. J. Ranft: Phys. Rev. D37 (1988) 1842
3. K. Werner: Phys. Lett. B208 (1988) 520
4. B. Anderson, G. Gustafson, B. Nilsson-Almquist: Nucl. Phys. B281 (1987) 289
5. M. Gyulassy: preprint CERN-Th 4794 (1987)
6. A. Capella, J. Tran Thanh Van: Z. Phys. C – Particles and Fields 38 (1988) 177
7. J. Ranft, S. Ritter: Z. Phys. C – Particles and Fields 20 (1983) 347
8. J. Ranft, S. Ritter: Z. Phys. C – Particles and Fields 27 (1985) 413
9. J. Ranft, S. Ritter: Z. Phys. C – Particles and Fields 27 (1985) 569
10. R. Albrecht et al. WA 80-Coll.: Phys- Lett. B199 (1987) 297
11. T. Akesson et al. Helios-Coll.: preprint CERN-EP/87-176 (1987)
12. A. Bamberger et al. NA 35-Coll.: Phys. Lett. B184 (1987) 271
13. J. Ranft: preprint CERN-TIS/Rp 219/PP (1988), submitted to Z. Phys. C – Particles and Fields
14. T.C. Awes et al.: Report on the Oak Ridge Workshop on Monte Carlo Codes for Relativistic Heavy-Ion Collisions, Seventh International Conference on Ultrarelativistic Nucleus-Nucleus Collisions, Lenox, Massachusetts, 1988
15. F. Corriveau et al. Helios-Coll.: Z. Phys. C – Particles and Fields 38 (1988) 15
16. C. De Marzo et al.: Phys. Rev. D26 (1982) 1019
17. F. Dengler et al.: Z. Phys. C – Particles and Fields 33 (1986) 187
18. J.E. Elias: Phys. Rev. D22 (1980) 13
19. W. Busza, R. Ledoux: Ann. Rev. Nucl. Part. Sci. 38 (1988) 119
20. R. Albrecht et al. WA 80-Coll.: Phys. Lett. B202 (1988) 596
21. A. Shor, R. Longacre: Phys. Lett. B218 (1989) 100
22. V.D. Toneev: private communication (1989)
23. M. Gyulassy, L.P. Csernai: Nucl. Phys. A460 (1986) 721
24. T. Rentzsch et al.: Mod. Phys. Lett. A2, 3 (1987) 193
25. S.Z. Belen'kji, L.D. Landau: Suppl. II, Ser. X, Nouvo Cimento 1 (1956) 15
26. A.E. Glassgold, W. Heckrotte, K.M. Watson: Ann. Phys. 6 (1959) 1
27. H.G. Baumgardt et al.: Z. Phys. A – Atomic Nuclei 273 (1975) 359
28. H.-Å. Gustafsson et al.: Phys. Rev. Lett. 52 (1984) 1590
29. H. Stöcker, W. Greiner: Phys. Rep. 137 (1986) 277
30. K.G.R. Doss et al.: Phys. Rev. Lett. 59 (1987) 2720
31. H.R. Schmidt et al. WA 80-Coll.: Z. Phys. C – Particles and Fields 38 (1988) 109
32. A. Baden et al.: Nucl. Instrum. Methods 203 (1982) 189
33. R. Albrecht et al. WA 80-Coll.: Report No. GSI-85-32, Gesellschaft für Schwerionenforschung, D-6100 Darmstadt (1985)
34. G.R. Young et al.: submitted to Nucl. Instrum Methods
35. W. Heck et al. NA 35-Coll.: Z. Phys. C – Particles and Fields 38 (1988) 19
36. K. Aleklett, L. Sihver, W. Loveland: Phys. Lett. B197 (1988) 34
37. L.M. Barbier et al.: Phys. Rev. Lett. 60 (1988) 405